

Direct observation of waveguide formation in $\text{KGd}(\text{WO}_4)_2$ by low dose H^+ ion implantation

C. A. Merchant^{a)} and J. S. Aitchison

Department of Electrical and Computer Engineering, University of Toronto, Toronto M5S 3G4, Canada

S. Garcia-Blanco

National Optics Institute (INO), Sainte-Foy, Québec G1P 4S4, Canada

C. Hnatovsky and R. S. Taylor

Institute for Microstructural Sciences, National Research Council, Ottawa K1A 0R6, Canada

F. Agulló-Rueda

Materials Science Institute of Madrid (CSIC), Cantoblanco, E-28049 Madrid, Spain

A. J. Kellock and J. E. E. Baglin

IBM Almaden Research Center, 650 Harry Road, San Jose, California 95120-6099

(Received 23 February 2006; accepted 20 July 2006; published online 14 September 2006)

In this letter, a direct measurement of a refractive index change in potassium gadolinium tungstate (KGW) created by a low-dose ion implantation of 1 MeV hydrogen ions is reported. The characterization was performed using both microreflectivity and Raman spectroscopy measurements. The microreflectivity results show both negative and positive changes in refractive index in the damage region when measuring refractive index along different polarization axes. Micro-Raman spectroscopy analysis shows preservation of the Raman characteristics of KGW in the nondamaged crystal regions. These results show that ion implantation in KGW has a great potential for fabricating waveguide structures in Raman-based photonic devices. © 2006 American Institute of Physics. [DOI: 10.1063/1.2340496]

Optical waveguide formation in crystals has been studied extensively for use in many applications, such as efficient and compact lasers, switches, couplers, and other integrated photonic devices. Potassium gadolinium tungstate [$\text{KGd}(\text{WO}_4)_2$] (or KGW) is a popular monoclinic crystal exhibiting high nonlinear refractive index, thermo-optical properties, and suitability as a rare-earth host material.¹⁻⁵ It is also a very promising Raman-active material, with strong Stokes lines at 768 and 901 cm^{-1} with respective linewidths of 7.8 and 5.9 cm^{-1} , and Raman gain coefficients of 6 cm/GW for both lines.^{6,7} There is great potential for the application of waveguides in KGW crystals, with recent research showing very promising application for all-optical generation, beam steering, and switching devices.⁸

Ion implantation of light, high energy ions in KGW, and other crystal materials offers a method of modifying the refractive index of the material in relatively well-defined areas, to a controlled depth, allowing for the formation of waveguide structures.^{9,10} Light ions with energies in the MeV range penetrate the material, losing energy, and slowing via electronic and nuclear interactions. As the energy of the ions penetrating the material becomes low enough, elastic nuclear collisions occur, causing atomic displacement of the lattice structure, which generally results in the decrease of refractive index of the material. This decrease in refractive index forms an optical barrier, where a guiding region is formed between the crystal surface and the damaged region. In some cases, an increase of refractive index is seen in crystals in the extraordinary index axis for low ion doses, due to bond compaction, ionic motion, or modified bond rearrangements.¹¹

There has been previous research into planar KGW waveguides formed by pulsed laser deposition of thin films of KGW on the surfaces of substrates;^{12,13} however, ion implantation allows fabrication of buried channel waveguides with precise control over core size, depth, and damage region thicknesses by varying the ion implantation energy and dose. Ion irradiation of KGW by swift heavy ions has been reported,¹⁴ however, the use of light ions such as H^+ and He^+ allows deeper penetration into the material, potentially allowing fabrication of waveguides at different depth levels. In order to understand and design optical waveguides fabricated by ion implantation in KGW, both the refractive index distribution induced by the ions and the Raman properties of the implanted waveguide region should be known. Most of the previous research on ion implantation in crystals used m -line experiments to indirectly infer the refractive index profile by measuring the dark modes of the waveguide. This letter presents direct measurement of the variation of refractive index induced in the different polarization axes using a microreflectivity setup. The structural modifications in the material due to ion implantation were also characterized by micro-Raman spectroscopy. The Raman measurements show that the crystalline properties of the material are maintained in the guiding region, therefore demonstrating the possibilities of using H^+ ion implantation for the fabrication of waveguides in KGW.

The undoped KGW sample was purchased from Passat Ltd., and was implanted as shown in Fig. 1 with 1 MeV H^+ ions at doses of 10^{14} , 10^{15} , 10^{16} , and 5×10^{16} ion/cm^2 without annealing. The three indices of refraction for the KGW crystal at 633 nm can be calculated from the appropriate Sellmeier coefficients to be 2.041 along the N_m axis, 2.095 along the N_g axis, and 2.011 along the N_p axis.⁴ The sample

^{a)}Electronic mail: clark.merchant@utoronto.ca

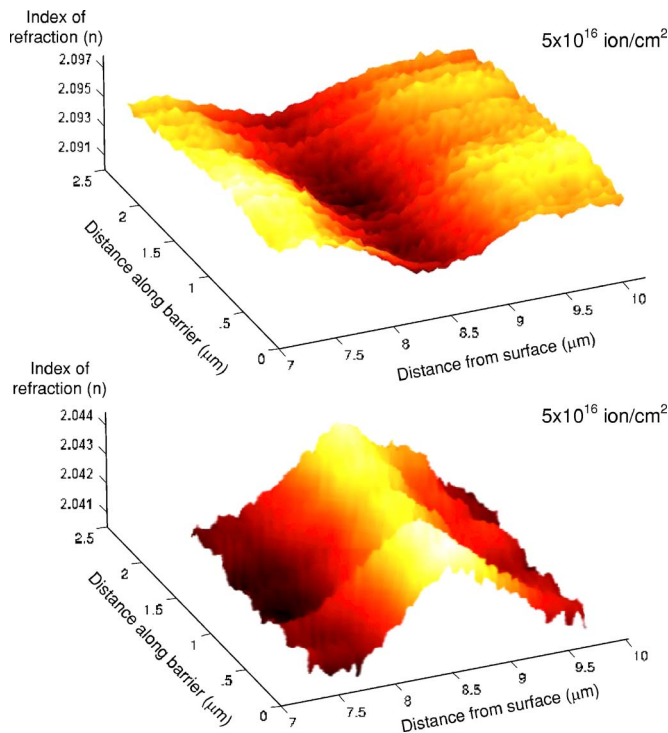


FIG. 1. (Color online) Microreflectivity area measurement around the damage region of the crystal illustrating the negative refractive index profile (top) for a beam polarized in the N_g direction, and the positive refractive index profile (bottom) for a beam polarized in the N_m direction.

was diced to separate dose regions and polished. Microreflectivity measurements were made along the $15 \times 0.5 \text{ mm}^2$ side of the crystal, aligned to measure either the N_m or N_g axes.

The microreflectivity measurements were carried out using a HeNe laser with a 632.8 nm wavelength and a maximum power of $\approx 1 \text{ mW}$ focused through a Carl Zeiss $50\times$ objective with numerical aperture=0.8 objective onto the sample.¹⁵ A polarizer and wave plate combination was used to control the polarization of the probe beam. The sample was placed on an XYZ piezoscanner, with a scan accuracy of approximately 1% of the scan size (scan size is typically 10–15 μm along each axis) and at each point the reflectivity of the sample was recorded.

The Fresnel formula relating the reflectivity R of the sample to its refractive index n can be written as

$$\Delta n = \frac{n(r)^2 - 1}{4} \frac{\Delta R}{R(r)}, \quad (1)$$

where $n(r)$ is the index of refraction and $R(r)$ is the reflectivity measured at point r on the surface. If there is a reference position where the index of refraction is known and the reflectivity can be measured, Eq. (1) can be rewritten in terms of this reference position as Eq. (2), where $n(r_{\text{ref}})$ is the index of refraction on a known reference location on the sample and $R(r_{\text{ref}})$ is the measured reflectivity at this location.

$$\Delta n = \frac{1}{4} (n(r_{\text{ref}})^2 - 1) \frac{R(r) - R(r_{\text{ref}})}{R(r_{\text{ref}})}. \quad (2)$$

The microreflectivity setup allows a spatial resolution of approximately 400 nm with an index of refraction variation of 1×10^{-4} .¹⁶ The different samples were measured and a dam-

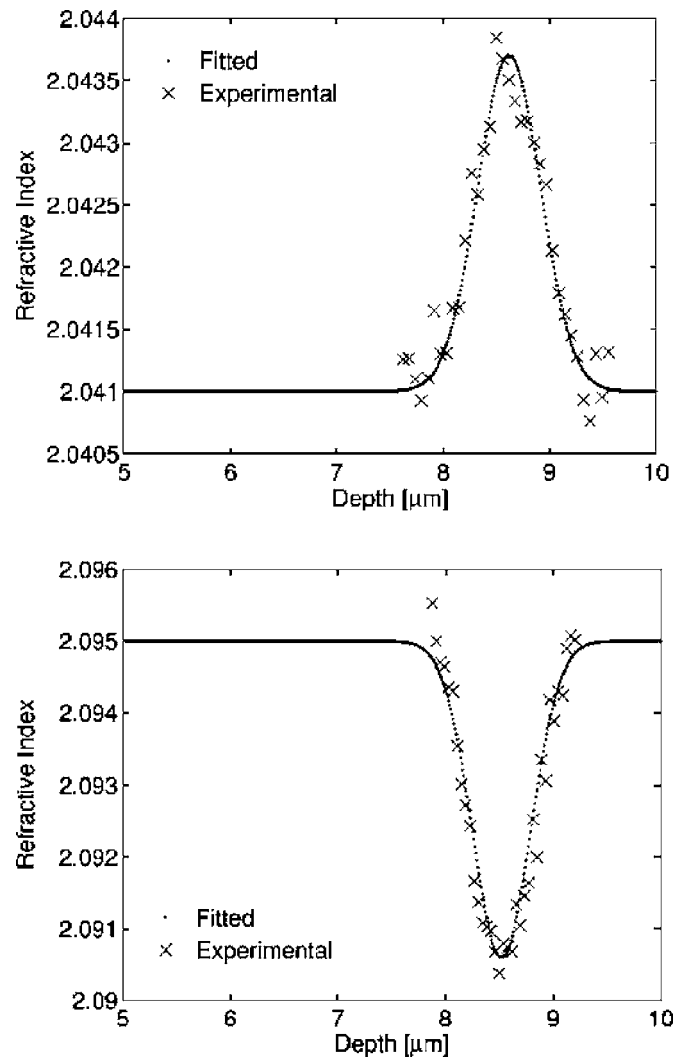


FIG. 2. Detailed microreflectivity measurement for a single scan line of the barrier region for the probe beam with polarization aligned to the N_m axis (top) and N_g axis (bottom) directions.

age region was found only in the sample with $5 \times 10^{16} \text{ ion/cm}^2$ dose. This damage region was measured at several locations along the crystal using polarizations along the N_m and N_g axes, over a $10 \times 10 \mu\text{m}^2$ window (256×256 data points) at a scan rate of 6.1 Hz. The refractive index profiles of the barrier for each polarization measurement are magnified and shown in Fig. 2. A peak negative refractive index change of approximately $\Delta n \approx -0.004$ (0.19%) was measured when the beam was polarized along the crystal N_g axis, and a positive refractive index change was measured to be $\Delta n \approx 0.003$ (0.15%) when measured with the beam polarization along the N_m axis. The index of refraction profile is roughly Gaussian in shape, with an approximate barrier width of 1–1.5 μm , with an error limited to the measurement capability of the system. Both the positive and negative index of refraction regions were measured with the microreflectivity setup to be approximately 8–9 μm from the edge of the crystal, with accuracy limited somewhat due to roll off of the reflectivity measurement attributed to limitations in polishing of the crystal. The measurements correlate well with results simulated using SRIM 2003 software package shown in Fig. 3, where simulations of the nuclear damage region behave approximately the same way as ex-

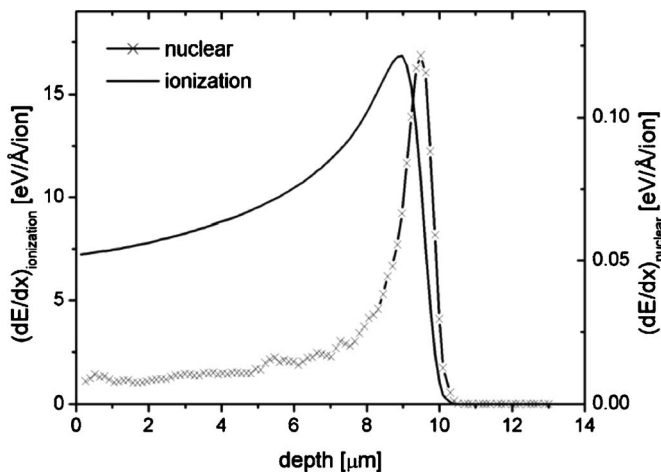


FIG. 3. SRIM simulations of the energy deposited by the 1 MeV H^+ ions inside the KGW by ionization and nuclear collision events.

perimental measurements of the refractive index barrier, within the measurement error of the system.

Micro-Raman measurements of the sample were taken using a Renishaw Ramascope 2000 micro-Raman instrument in confocal configuration ($13 \mu\text{m}$ wide slits and 4 pixels binning of the charge-couple device). The excitation source was an Ar^+ laser at 514.5 nm and 10 mW power. Figure 4 shows the evolution of the intensity of the peak at 901 cm^{-1} as a function of the distance from the surface of the sample for implant doses varied from 0 to $5 \times 10^{16} \text{ ion/cm}^2$. Two main effects can be observed, a shift of the position of the barrier towards the surface of the sample as the dose is increased, and an asymmetric widening of the barrier. Both effects can be explained by the asymmetric shape of the electronic stopping power of the ions inside the KGW material, as shown in Fig. 3. As the dose increases, more effective amorphization is produced on the side of the barrier closer to the surface, therefore shifting its position towards the surface. As a consequence, by increasing the ion dose, the width of the core of the waveguide can be varied. Finally, Fig. 4 shows that, even for high doses, the Raman behavior of the material in the region of the core of the waveguide is preserved for the N_g axis, although for the N_m axis the waveguide core would be found in the damage region, limiting the effectiveness of Raman processes. The damage region is found to be approximately $8.5 \mu\text{m}$ from the surface, shown by a decrease of the intensity of the peak. This result is consistent with the microreflectivity results showed above for the $5 \times 10^{16} \text{ ion/cm}^2$ dose.

This letter has shown a direct observation of both negative and positive index of refraction changes in the KGW crystal when exposed to a low dose of $1 \text{ MeV } H^+$ ions. The negative change in refractive index barrier for the N_g polarization allows for modes to guide in an undamaged region of the crystal, preserving Raman and nonlinear refractive index

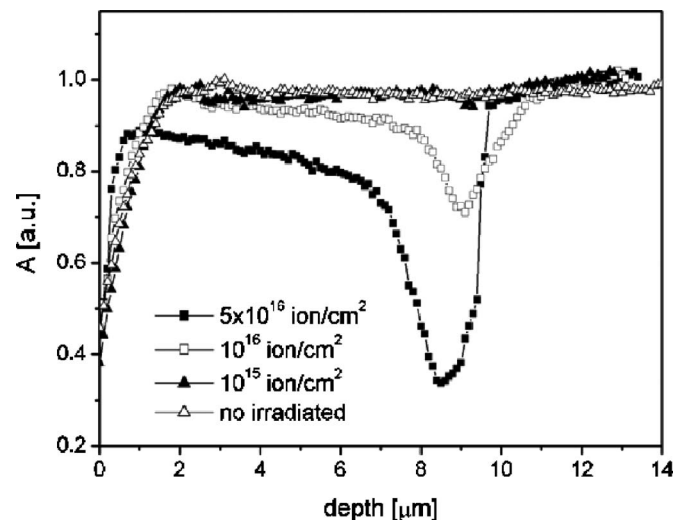


FIG. 4. Evolution of the intensity of the Raman peak at 900 cm^{-1} as a function of depth inside the KGW for different ion doses.

properties. The presence of the positive change in refractive index for the N_m polarization moves the waveguide core into the damage region of the crystal, and therefore the material properties such as the efficient Raman generation and high n_2 value will be affected; however, possible novel filter or switching applications could be used with this phenomenon.

¹S. V. Kurbasov and L. L. Losev, *Opt. Commun.* **168**, 227 (1999).

²P. A. Atanasov, T. Okato, R. I. Tomov, and M. Obara, *Thin Solid Films* **453–454**, 150 (2004).

³C. Tu, M. Qiu, J. Li, and H. Liao, *Opt. Mater. (Amsterdam, Neth.)* **16**, 431 (2001).

⁴M. C. Pujol, M. Rico, C. Zaldo, R. Sole, V. Nikolov, X. Solans, M. Aguilo, and F. Diaz, *Appl. Phys. B: Lasers Opt.* **68**, 187 (1999).

⁵A. Major, I. Nikolakakos, J. S. Aitchison, A. I. Ferguson, N. Langford, and P. W. E. Smith, *Appl. Phys. B: Lasers Opt.* **77**, 433 (2003).

⁶A. S. Grabtchikov, A. N. Kuzmin, V. A. Lisinetskii, G. I. Ryabtsev, V. A. Orlovich, and A. A. Demidovich, *J. Alloys Compd.* **300–301**, 300 (2000).

⁷A. Z. Grasiuk, S. V. Kurbasov, and L. L. Losev, *Opt. Commun.* **240**, 239 (2004).

⁸C. A. Merchant, I. V. Mel'nikov, and J. S. Aitchison, in *Nonlinear Guided Waves and Their Applications Topical Meeting on CD-ROM* (The Optical Society of America, Washington, DC, 2005), ThB18.

⁹G. Gotz and H. Karge, *Nucl. Instrum. Methods Phys. Res.* **209/210**, 1079 (1983).

¹⁰P. D. Townsend, *Vacuum* **34**, 395 (1984).

¹¹J. Rams, J. Olivares, P. J. Chandler, and P. D. Townsend, *J. Appl. Phys.* **87**, 3199 (2000).

¹²J. Lancok, C. Garapon, V. Vorliceck, M. Jelinek, and M. Cernansky, *Opt. Mater. (Amsterdam, Neth.)* **28**, 360 (2006).

¹³P. A. Atanasov, M. Jimenez de Castro, A. Perea, J. Perriere, J. Gonzalo, and C. N. Afonso, *Appl. Surf. Sci.* **186**, 469 (2002).

¹⁴A. Garcia-Navarro, J. Olivares, G. Garcia, F. Agullo-Lopez, S. Garcia-Blanco, C. Merchant, and J. S. Aitchison, *Nucl. Instrum. Methods Phys. Res. B* **249**, 177 (2005).

¹⁵S. G. Blanco, J. S. Aitchison, C. Hnatovsky, and R. S. Taylor, *Appl. Phys. Lett.* **85**, 1314 (2004).

¹⁶R. S. Taylor, C. Hnatovsky, E. Simova, D. M. Rayner, M. Mehandale, V. R. Bhardwaj, and P. B. Corkum, *Opt. Express* **11**, 775 (2003).